Research Article : Open Access

DOI: 10.35840/2631-5033/1871

VIBGYOR ePress

International Journal of
Earth Science and Geophysics

Development of an Enzyme-Induced Calcite Precipitation Method Aimed to Improve the Shielding Property of Porous Rocks and Assessment of its Effect

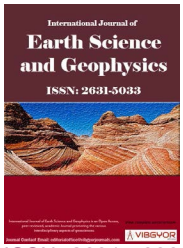

ISSN: 2631-5033

Eldan ARKIN[1*], Takumi MORI[2], Ren HIMENO[1], Atsushi SAINOKI[3] and Akira SATO[3]

[1]*Graduate School of Science and Technology, Kumamoto University, 860-8555, Japan*

[2]*West Japan Engineering Consultants, 810-0004, Japan*

[3]*Graduate School of Advanced Science and Technology, Kumamoto University, 860-8555, Japan*

Abstract

This study investigated the Enzyme-Induced Calcite Precipitation (EICP) method for enhancing water-shielding properties in porous rock formations while addressing its relevance to carbon capture and storage (CCS) initiatives. EICP involves precipitating calcium carbonate within the aquifer to block pores structures in the rock mass. The action of the urease, a urea-degrading enzyme, was investigated during this process. Calcium carbonate was precipitated by introducing a solution comprising urea, calcium chloride, and urease into the rock pores. We used different concentrations of solutions to assess the precipitation time and amount of precipitation during the experiment. Berea sandstone and Ainoura sandstone were selected as representative porous rock samples. The EICP method was applied to dried rock samples, and the resulting density changes were visualized using an industrial X-ray CT scanner. Significant precipitation was observed within the Berea sandstone, while less precipitation occurred in the Ainoura sandstone. Furthermore, a one-dimensional permeability test was conducted to evaluate the water-shielding properties quantitatively. The intrinsic permeability of both the Berea and Ainoura sandstones decreased when the EICP method was applied, with the decrease being more pronounced in the Berea sandstone. After three applications of EICP, the intrinsic permeability of Berea sandstone decreased by approximately 1/10, while the Ainoura sandstone exhibited minimal changes in intrinsic permeability with varying application numbers. The results highlight the potential of EICP as a viable approach for enhancing water-sealing capabilities in geotechnical and environmental applications, which offers the potential for carbon sequestration within the rock formations, contributing to the efforts to mitigate climate change and reduce greenhouse gas emissions.

Keywords

Calcium carbonate, Enzyme-induced calcite precipitation, Sandstone, Industrial X-ray CT scanner, Permeability

Introduction

In recent years, global warming has been progressing worldwide due to greenhouse gases, such as carbon dioxide (CO_2), emitted by the mass consumption of fossil fuels, such as petroleum and coal. Therefore, interest in SDGs (Sustainable Development Goals) has recently spread worldwide, emphasizing measures to combat environmental problems such as climate change. Therefore, CO_2

***Corresponding author:** *Eldan ARKIN, Graduate School of Science and Technology, Kumamoto University, 860-8555, Japan*

Accepted: August 19, 2023; **Published:** August 21, 2023

Citation: ARKIN E, MORI T, HIMENO R, SAINOKI A, SATO A (2023) Development of an Enzyme-Induced Calcite Precipitation Method Aimed to Improve the Shielding Property of Porous Rocks and Assessment of its Effect. Int J Earth Sci Geophys 9:071

underground storage technology (CCS, CO_2 Capture and Storage) is attracting attention as one of the technologies aimed at reducing the concentration of CO_2 in the atmosphere. CCS is a technology that reduces emissions by storing CO_2 that has been separated and recovered from large-scale sources, such as factories and power plants, in an underground aquifer. With this initiative, 1 million tons of CO_2 have been stored underground annually in Sleipner in Norway and Weyburn in Canada [1-4]. In Japan, an experiment of underground storage is being attempted in Nagaoka, Niigata Prefecture, and a large-scale CCS test is being conducted in Tomakomai, Hokkaido, with the target cumulative amount of CO_2 injected of 300,000 tons. CCS has become a key part of the Dutch climate policy in the Netherlands and is expected to contribute up to 8 Mt of CO_2 reduction [5]. In India, a new method using porous organic frameworks has substantial potential for CO_2 capture and short-term storage applications [6]. Australia has also utilized CO_2 and storage, with CO_2 storage of 10-50,000t CO_2 per 3-5 million tons per annum for the Gorgon LNG Project and up to 10 million tons of CO_2 per annum for the Monash Project [7]. In 2009, a five-year collaboration between researchers in the United States and China reported that China has a large and geographically dispersed theoretical deep geologic CO_2 storage capacity of over 2,300 Mt CO_2 in onshore basins, with an additional 780,000 Mt CO_2 in offshore basins near the coast. Deep saline-filled sedimentary basins account for more than 99% of the total calculated storage capacity [8]. The Russian Federation has also discussed the possibility of mechanisms affecting the preservation of injected-gas structural or stratigraphic trapping, hydrodynamic trapping, solubility trapping, and mineral trapping, which provide the required level of injection safety [9]. Montana State University investigated the potential of using microorganisms to enhance carbon capture and storage via mineral trapping and solubility trapping [10]. Stanford University has also studied the capture and storage technique and whether sufficient potential capacity exists for storage in geologic formations, described the physical mechanisms that can prevent the escape of CO_2 from the subsurface, delineated methods for monitoring the movement of CO_2 in the subsurface and detecting leaks, and described field experience with CO_2 injection [11]. A novel approach presented by Michigan University uses a sodium carbonate solution to first capture CO_2 from post-combustion flue gas streams, which is then reacted with an alkaline industrial waste material under ambient conditions to regenerate the carbonate solution and permanently stored in the form of a value-added carbonate mineral [12]. Florida International University invented methods for CO_2 capture, which provide systems and methods for capturing CO_2 in a cyclic process of mechanochemical reactions using mill rotation. These systems and methods employing CO_2 capture reactions in the carbonation-calcination cycles are suitable for use in the iron, steel, and non-steel industries to reduce CO_2 emissions into the atmosphere [13].

In CCS, leakage of CO_2 in the vertical direction can be prevented by a shielding layer (cap lock). However, in the horizontal direction of the aquifer, CO_2 may diffuse or leak into inappropriate places, making it essential to improve the water's impermeability to ensure safety. Therefore, in this study, we focused on calcium carbonate, which is a weakly soluble crystal, and aimed to improve its impermeable properties with the precipitation of calcium carbonate in the voids in the bedrock. In the field of ground engineering, research on ground improvement technology using the precipitation of calcium carbonate crystals with the aid of the metabolic activity of microorganisms in soil is progressing. Research is also being conducted on small-scale CCS, investigating the potential of microorganisms to enhance carbon capture and storage via mineral and solubility trapping [14]. Sealing technologies are also used as mitigation strategies for cap rocks, which is critical in the long-term security of geologically stored CO_2 [15]. Novel engineering applications have mainly focused on urease-aided calcium carbonate mineralization and reviewed its advantages and limitations compared with conventional techniques [16]. Therefore, in our laboratory, we applied calcium carbonate precipitation technology to the bedrock, which was infiltrated with urease, a urea-degrading enzyme, in an aqueous solution of urea and calcium chloride (hereinafter referred to as grout material). In this study, the enzyme-induced calcite precipitation applied to rock samples using grout materials with various formulations led to an improvement in the water impermeability evaluation.

Enzyme-Induced Calcite Precipitation method

is an innovative ground improvement technique that involves calcium carbonate precipitation via hydrolysis of urea into ammonium and carbonate catalyzed by the urease enzyme. EICP is widely used in soil stabilization to improve the strength and stiffness of soil and mitigate [17-20]. In our case, we used this method on rock samples to analyze and evaluate the permeabilities and improve the shielding properties.

The purpose of this study was to determine the optimum blending design of grout material using the enzyme-induced calcite precipitation method and to quantitatively evaluate the effect of improving water impermeability by closing the voids inside the rock when the enzyme-induced calcite precipitation method was applied. The main evaluation methods were an evaluation using a one-dimensional water permeability test for the quantitative evaluation of impermeable properties and a bulk evaluation using an industrial X-ray CT scanner of the void blockage with calcium carbonate.

X-ray imaging has been applied in biomedicine down to the submicron scale for at least a decade. In contrast, it has only recently been applied to rock studies, and few researchers have realized its value and potential [21]. In recent years, X-ray image analysis techniques have been extensively studied in various fields. To obtain CT images, several image processing methods must be considered, such as noise reduction and segmentation [22]. The most important part of evaluating the physical properties of rock samples is pore and grain phase separation, which significantly affects the physical property measurements of the rock using these techniques [23]. Additionally, pore-scale modeling with a reconstructed rock microstructure has become a dominant technique for fluid flow characterization in rocks owing to the technological improvements in X-ray computed imaging [24]. In addition, pore-scale X-ray imaging plays a crucial role in detecting the physical properties of rock samples and permeability in steady-state and unsteady-state flows [25]. In geological research, X-ray micro tomography imaging has also been implemented for the quantitative analysis of volcanic rocks [26]. X-ray image analysis has also been used to quantitatively characterize the size distribution and volume contribution of pore fractures in coal at three cohesive scales [27]. Finally, a clear understating of the flows in porous media is vital for investigating geological CO_2 storage, because the maximum CO_2 saturation is determined by the porosity distribution. Additionally, we need to clearly understand the two-phase flows in porous media to predict the continuum-scale processes that occur during CO_2 storage in deep saline aquifers. Several simulation studies have reported the importance of characterizing the relative permeability governing the CO_2 distribution, depending on the surface tension associated with the combined forces arising at the interface separating two or more phases [28]. Furthermore, pore networking modeling offers an efficient means of examining the complex variety of microscopic processes affecting the subsurface migration of CO_2 injected for storage [29].

The objectives of this study were to investigate the optimal mixing design of grouting materials in the enzyme-induced calcite precipitation (EICP) method and to quantitatively evaluate the effect of this method on improving impermeability by blocking pores within the rock. While EICP is primarily used for soil stabilization, in this case, we applied it to porous rock to enhance impermeability. Specifically, we varied the concentrations of reactants (urea and calcium chloride) and catalyst (urease) to produce sufficient precipitation materials capable of infiltrating the rock sample and precipitating within its pore structure to enhance its impermeable properties. The main evaluation methods included one-dimensional permeability tests to quantitatively assess impermeability properties and the use of an industrial X-ray CT scanner to analyze bulk calcium carbonate void closure phenomena.

Experimental Procedure

In this study, a one-dimensional water permeability test and X-ray image analysis were performed to evaluate the water impermeability when the enzyme-induced calcite precipitation was applied. The details of the rock samples were described, and the one-dimensional permeability test device used, and the industrial X-ray CT scanner is explained below.

Methodology for processing rock samples and equipment for one-dimensional permeability testing

In this study, Berea and Ainoura sandstones were selected as representative rock samples.

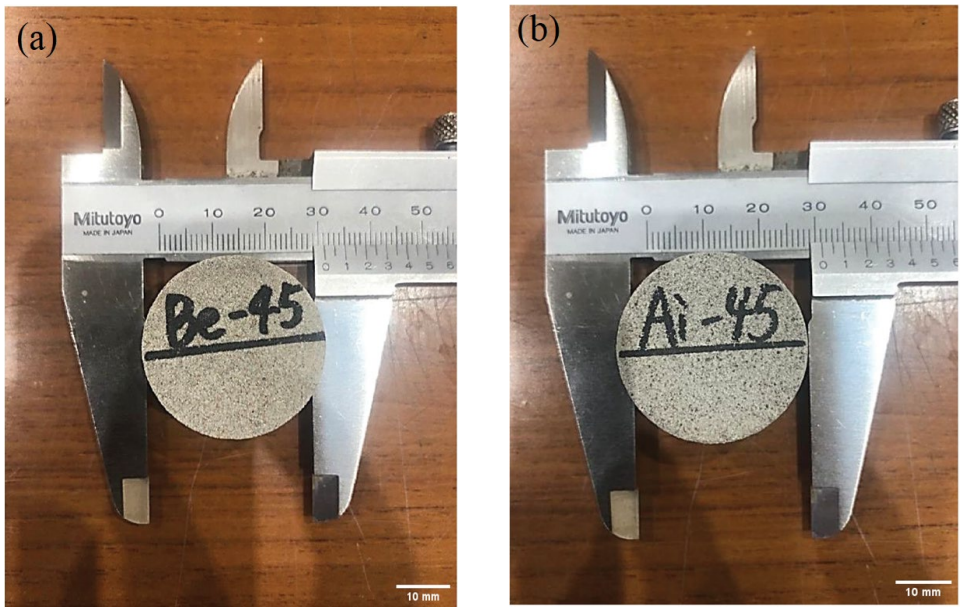

Figure 1: Rock samples: a) Berea sandstone; b) Ainoura sandstone.

The Berea sandstones used in our experiments exhibited an intrinsic permeability ranging from approximately 10^{-15} m^2 to 10^{-14} m^2, with a porosity of approximately 15%. The Ainoura rock samples' intrinsic permeability ranged from around 10^{-18} m^2 to 10^{-17} m^2, accompanied by a 10% porosity. Berea sandstone is distributed throughout Ohio and is famous as an oil and natural gas reservoir. It is a fine-grained sandstone with excellent porosity and permeability, making it a popular choice for laboratory experiments and research studies related to petroleum and geotechnical engineering. Berea sandstone is used as a model test sample by numerous engineers in North America and is called the world standard. Ainoura sandstone is widely distributed around Sasebo City, Nagasaki Prefecture. It is known for its distinctive light gray-to-white color and fine-grained texture. In addition, it has been suggested that the flow path of the Ainoura sandstone is selective, with the flow rate of a portion of the rock predominating.

Figure 1 shows the rock sample was formed by removing the core from a rectangular parallelepiped block as a cylindrical shape. In this study, samples for the CT imaging and one-dimensional permeability tests were prepared with sizes suitable for each application. For the CT imaging, the rock samples were prepared with different sample diameters according to the scanner used, and for the one-dimensional water permeability test, the sample diameter was 30 mm, with a height of 30 mm.

Displayed in Figure 2 is a rock sample that has been prepared exclusively to conduct a one-dimensional experimental test. A rock sample was prepared with a porous rock material installed on one end surface, allowing water to permeate through it. A drain pump was also installed at this end surface to facilitate water discharge. To prevent water leakage from unintended areas, the sample was coated with epoxy resin, serving as a protective barrier. During the experiment, water was introduced onto the open surface of the rock sample. The porous material allowed water to permeate into the internal structure of the rock, which was efficiently drained out through the installed pump, enabling precise control and monitoring of water flow throughout the experiment.

The laboratory setup for conducting the one-dimensional permeability testis illustrated in Figure 3. An ISCO syringe pump 500D (Nikkaki Bios Co., Ltd.) was used for the test. With this device, the pressure was able to be set to 0-25 MPa, and the flow rate was able to be set to 0.001-204 mL/min. The test was performed by selecting either the constant flow rate condition or the constant pressure condition. The pressure vessel used was a CFRP (Carbon reinforced plastic) pressure vessel developed in our laboratory.

In the first step, the processed rock sample was completely saturated with water and placed in a pressure vessel, and then a one-dimensional

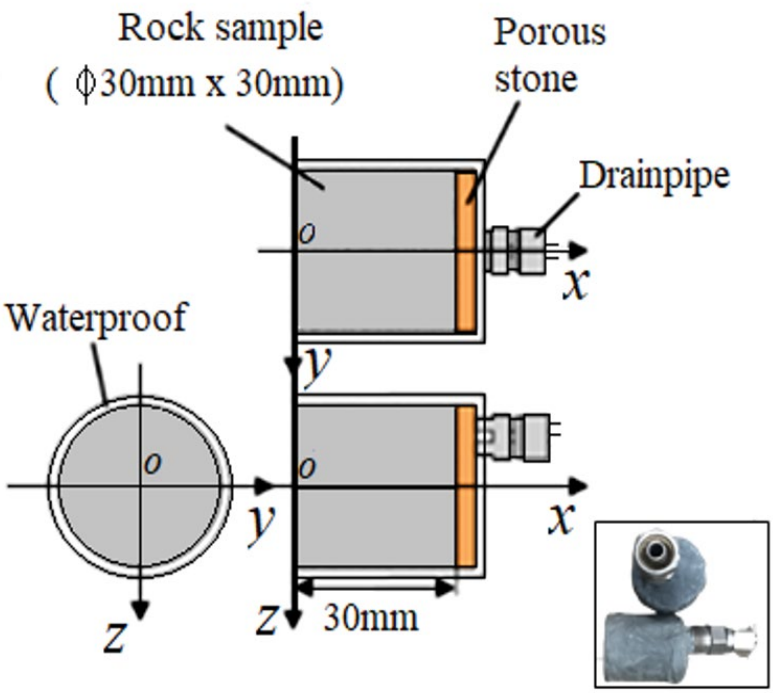

Figure 2: Processing diagram of rock sample for permeability test.

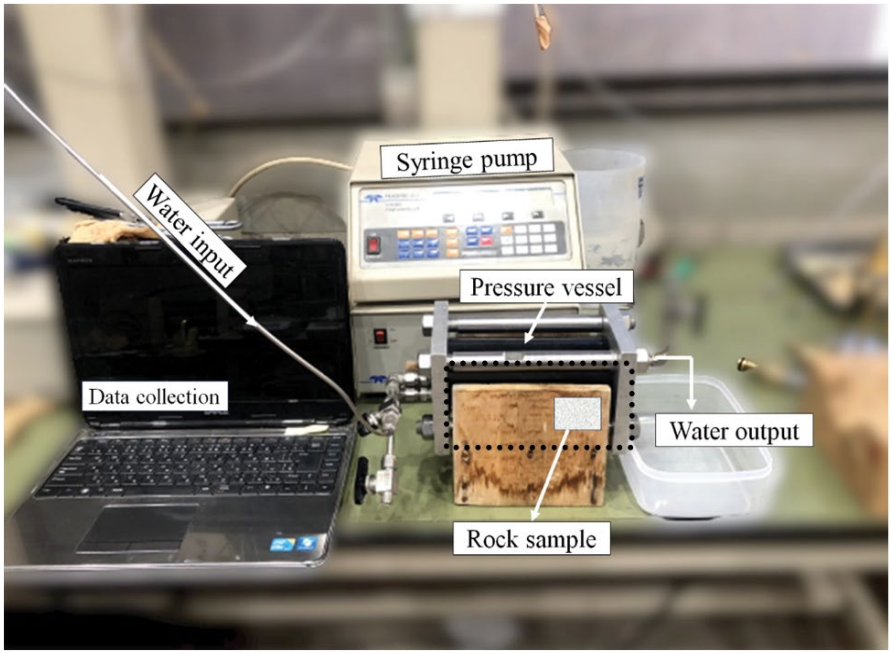

Figure 3: Laboratory setup for conducting one-dimensional permeability test.

permeability test was conducted using water as the working fluid. For the test conditions, it is generally easy to apply a constant flow rate condition for a sample with a large intrinsic permeability and a constant pressure condition for a sample with a small intrinsic permeability; therefore, we applied an inflow rate of 2 mL/min for the Berea sandstone. The Ainoura sandstone was subjected to a one-dimensional permeability test under a constant flow rate and constant pressure conditions with an inflow pressure of 2 MPa. The experiment was conducted assuming that the pressure on the outflow side was atmospheric. The pressure approached a constant value with time under constant flow rate conditions; therefore, the intrinsic permeation rate k was evaluated with

the pressure at the steady state. Additionally, the flow rate approached a constant value with time under constant pressure conditions; therefore, the intrinsic permeation rate k was evaluated using the inflow of water when the steady state was reached. The test results are described in Section 4.

Analysis using X-ray CT scanner

First, an outline of the industrial X-ray CT scanner was provided. Kumamoto University started operating an industrial X-ray CT scanner in 1997 and updated it to a new system (TOSCANNER-200RE) in 2006. However, as of December 2020, the operation of the industrial X-ray CT scanner ended. The X-ray laboratory used in this study was completely shielded with lead, and all the operations, other than placing the subject on the sample table, were performed outside the laboratory. This device had a maximum output of 300 kV/2 mA and photographed the object using tomography. The thickness could be selected from 6 types: 0.3 mm, 0.5 mm, 1 mm, 2 mm, 3 mm, and 4 mm.

Examination of Optimum Composition of Grout Material in Enzyme-Induced Calcite Precipitation

Before evaluating the void blockage inside the rock when it was infiltrated with the grout material using Berea sandstone and Ainoura sandstone, this chapter examines the optimum composition of the grout material to be used to infiltrate the target rock sample.

Basics of enzyme-induced calcite precipitation method

Mineral precipitation can drastically alter a reservoir's ability to transmit mass and energy during various engineering/natural subsurface processes, such as geothermal energy extraction and geological CO_2 sequestration, and plays a critical role in several energy-related applications. Furthermore, minerals precipitate as scales in the pore structure near wellbores and significantly reduce the permeability of the porous formation [30,31].

Before examining the application conditions of the enzyme-induced calcite precipitation method, the basic concept of the enzyme-induced calcite precipitation method will be described. The basic idea of the enzyme-induced calcite precipitation method is to inject an ionic chemical solution into the bedrock and combine the metal (cations) and carbonate (anions) ions contained in the chemical solution to form weakly soluble crystals, such as calcium carbonate ($CaCO_3$), that are deposited inside the voids of the porous rocks. This method improves the water impermeability of the bedrock by blocking the inside of the void or narrowing the void space. Calcium chloride ($CaCl_2$) was used as the calcium ion source and urea ($CO(NH_2)_2$) was used as the carbonate ion source to precipitate calcium carbonate. Furthermore, urease, which is an enzyme, was used as a catalytic substance for promoting urea hydrolysis.

The calcium carbonate precipitation reaction in the enzyme-induced calcite precipitation method is given by the following reaction formula:

$$\left(CO\left(NH_2\right)_2\right)+3H_2O \xrightarrow{\text{Urease}} 2NH_4^{+}+2OH^{-}+CO_2$$

$$CO_2+H_2O \leftrightarrow H_2CO_3$$

$$H_2CO_3 \leftrightarrow HCO_3^{-}+H^{+}$$

$$HCO_3^{-} \leftrightarrow CO_3^{2-}+H^{+}$$

$$CaCl_2 \leftrightarrow Ca^{2+}+2Cl^{-}$$

$$Ca^{2+}+CO_3^{2-} \rightarrow CaCO_3 \downarrow$$

The enzyme-induced calcite precipitation method applies this phenomenon to the voids in the bedrock which possibly clogs or reduces the pore space of rock samples.

Key considerations for implementing the enzyme-induced calcite precipitation method

When implementing the enzyme-induced calcite precipitation method in a rock mass, crucial factors must be taken into consideration. Firstly, the amount of calcium carbonate precipitated needs to be carefully evaluated. If the quantity of calcium carbonate deposited in the voids of the bedrock is insufficient, the voids will not be adequately blocked, resulting in no improvement in water properties. Secondly, the precipitation time of the calcium carbonate must be taken into account. If the calcium carbonate precipitates too quickly, it may occur before the grout material effectively infiltrates the site, and the deposition of calcium carbonate over a wide area will be limited. Therefore, it is important to deposit an appropriate amount of calcium carbonate in the bedrock voids and design a grout material composition that

requires sufficient precipitation time as much as possible. By considering these factors, we have determined the optimal composition of the grout materials.

Design of grout material considering $CaCO_3$ precipitation amount and precipitation time

When determining the composition of the grout materials, it is necessary to evaluate the precipitation amount and time of calcium carbonate in the grout material. Therefore, in this study, the calcium ion (Ca^{2+}) concentration was measured using an electrode-type calcium ion meter (Tokyo Kagaku Kenkyusho Co., Ltd.), and the amount of calcium carbonate precipitation and precipitation time were calculated.

The evaluation based on the Ca^{2+} concentration was based on the idea that the amount of precipitated calcium carbonate increases as the Ca^{2+} concentration in the grout material decreases. The precipitation efficiency was calculated from the data obtained by actual ion measurements, and the value was converted into the amount of $CaCO_3$ precipitation per 1L of grout material. Additionally, the concentration of Ca^{2+} during the blending process can be monitored using an electrode-type calcium ion meter. Precisely, at 150 minutes, the concentration of Ca^{2+} was measured at 700 mg/L, indicating that 20% of Ca^{2+} remained available for further calcium carbonate generation. At this time point, a precipitation material of 7.2 g/L was produced. Figure 4 provides a graph of the changes

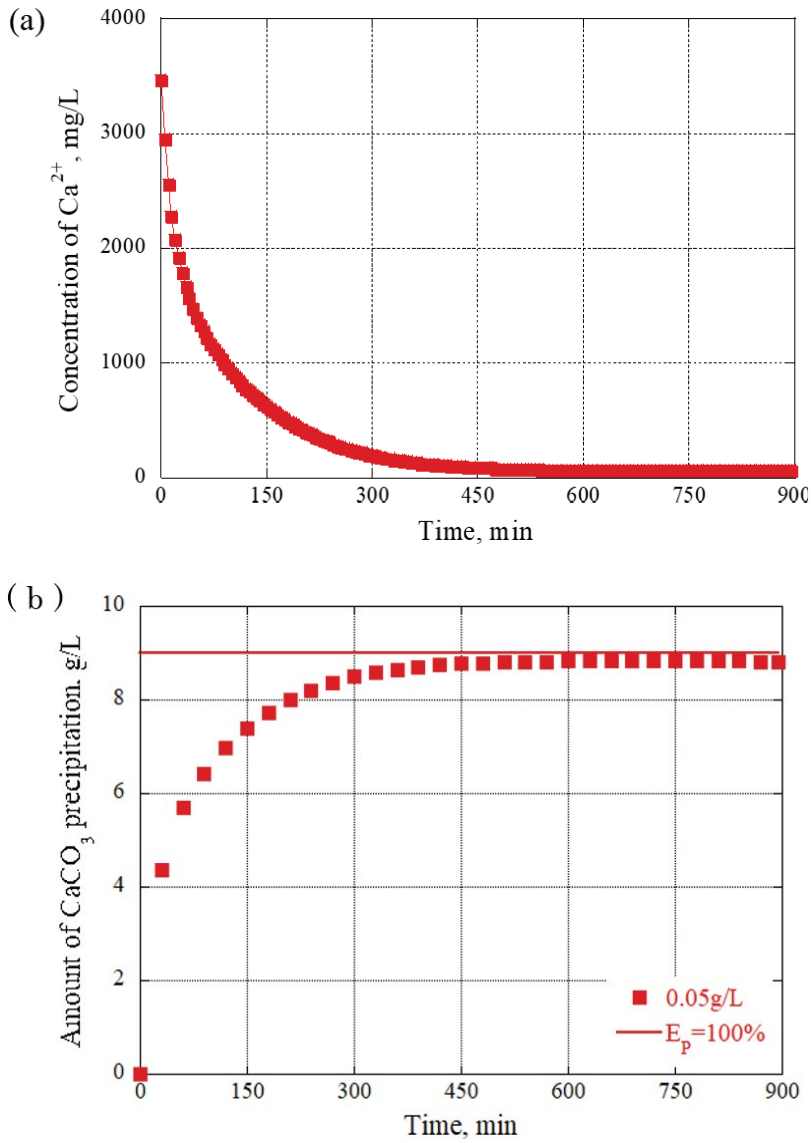

Figure 4: Example of Ca^{2+} measurement experiment results method, a) Changes in Ca^{2+} concentration in grout material over time; b) Changes in $CaCO_3$ precipitation per liter of grout material over time.

over time obtained from the calculation results. The precipitation efficiency EP = 100% in the figure indicates that all the calcium ions in the grout material were replaced with calcium carbonate crystals.

In this study, we prepared 300 mL of grout material prepared with the concentrations of urea and calcium chloride of 0.03 mol/L, 0.09 mol/L, and 0.15 mol/L, which were within the measurement range of the calcium ion meter, and calcium in a room temperature environment. Ion measurements were also carried out. Three types of ureases were prepared for use in this study: 490 u/mg urease (manufactured by Tokyo Kasei), 200 u/mg urease (manufactured by Toyobo Biochemical), and 2 u/mg urease (manufactured by Sigma-Aldrich Japan). 1 u is the amount of enzyme that converts 1 µmol of the substrate in 1 min at pH 7.0. In other words, when the same amount of urease was added, 490 u/mg urease molecules had the highest enzymatic activity and the highest reaction rate. On the other hand, 2 u/mg urease has the lowest enzyme activity and a lower reaction rate.

To verify how the urease concentration affected the precipitation amount and time of calcium carbonate, the urea, and calcium chloride concentrations were fixed, and the concentrations of urease were varied. Figure 5 shows the results of calculating the amount of $CaCO_3$ precipitates by fixing the urea and calcium chloride concentrations to 0.09 mol/L. Quantitatively, the concentrations of urease at 0.01g/L and 0.07 g/L demonstrated a tendency for rapid precipitation material generation compared to 0.05 g/L. Conversely, with a concentration of 0.03 g/L, there was an insufficient amount of precipitation generated, resulting in a gradual generation of precipitation materials compared to 0.05 g/L. Urease acts as a catalyst and plays a role in increasing the efficiency of reactions or providing the necessary energy for the continuation of chemical reactions. In this case, after 15 hours, as the urease concentration decreased, the efficiency of the reaction became less active, resulting in a decrease in the amount of $CaCO_3$ precipitation. Thus, the urease concentration in the grout material exhibited a significant influence on both the amount and time of $CaCO_3$ precipitation.

Next, to verify how the concentrations of urea and calcium chloride affected the precipitation amount and time of calcium carbonate, the urease concentration was fixed, and solutions with different concentrations of urea and calcium chloride were prepared. Figure 6 shows the changes in calcium carbonate precipitation over time with the grout materials prepared with urease concentrations of 0.05 g/L, respectively. At the 150-minute mark, a concentration of 0.09 mol/L of urea and calcium chloride produces 7.8 g/L of precipitation materials, which is significantly lower compared to the 12 g/L

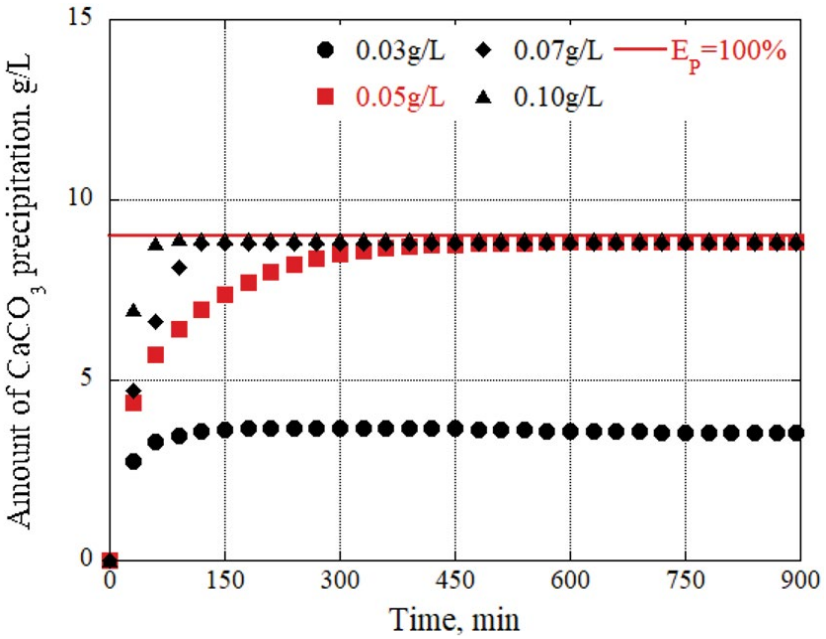

Figure 5: Changes in $CaCO_3$ precipitation per liter of grout material at 0.09 mol/L urea and $CaCl_2$ over time.

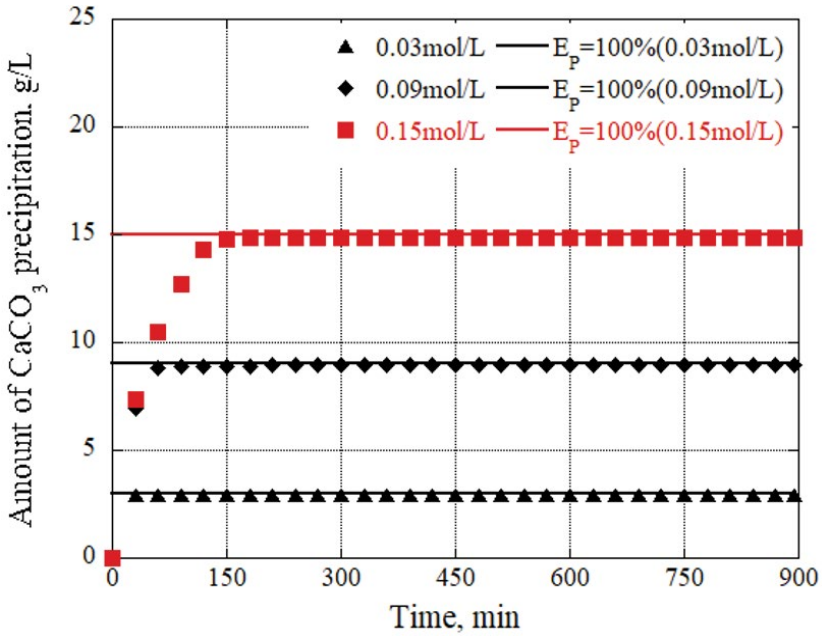

Figure 6: Changes in $CaCO_3$ precipitation per liter of grout material at 0.05 g/L urease concentration over time.

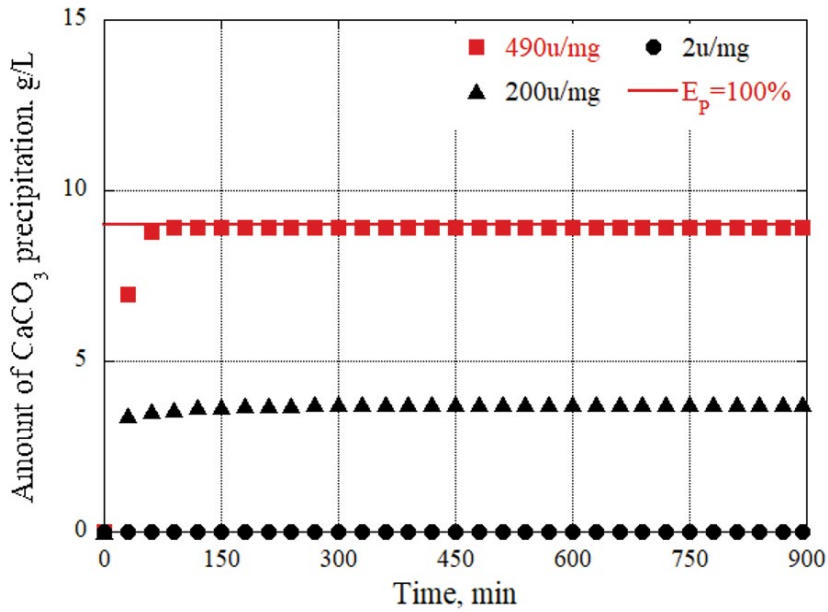

Figure 7: Changes in $CaCO_3$ precipitation per liter of grout material at different enzyme activity.

generated by the 0.15 mol/L concentration. This indicates that the formation of calcium carbonate is higher when using a urea and calcium chloride concentration of 0.15 mol/L, as opposed to other concentration levels. In general, the concentrations of urea and calcium chloride also have a significant impact on the amount of precipitation and precipitation time.

We also conducted experiments using three types of ureases with different enzyme activities. First, as an example, a grout material in which the urea and calcium chloride concentrations were fixed at 0.09 mol/L and the urease concentration was adjusted to 0.10 g/L using 490 u/mg urease, and the urease concentration using 200 u/mg urease. Figure 7 shows the results of changes in $CaCO_3$ precipitation in a total of three solutions: a grout material prepared to 0.10 g/L, a urease concentration adjusted to 0.10 g/L using 2 u/mg urease, and a total of three solutions.

In this experiment, a grout material was used with fixed concentrations of urea and calcium chloride at 0.09 mol/L. The concentration of urease was adjusted to 0.10 g/L using two different types of urease enzymes: One with an activity of 490 u/mg urease and the other with 200 u/mg urease. The results of the experiment are based on the changes in $CaCO_3$ precipitation observed in different solutions: grout material with a urease concentration of 0.10 g/L using 490 u/mg urease. grout material with a urease concentration of 0.10 g/L using 200 u/mg urease. Figure 7 presents the outcomes of three solutions regarding $CaCO_3$ precipitation. Additionally, calcium carbonate did not precipitate when 2 u/mg of urease was used. This is because the enzyme activity of 2 u/mg urease was only approximately 1/250 of that of 490 u/mg urease, so the amount of enzyme in the grout material was insufficient. In other words, in this study, if the same enzymatic activity as the grout material using 490 u/mg urease was expected, the urease concentration will be 25 g/L, which is approximately 250 times the urease concentration (0.10 g/L) using 2 u/mg urease. Therefore, to evaluate the $CaCO_3$ precipitation amount and time using urease with different enzyme activity, it was necessary to consider both the enzyme activity and concentration of the urease in the grout material and use new parameters. Therefore, the urease enzyme amount (u/L) per 1 L of grout material was calculated. As an example, the amount of urease enzyme per liter of grout material prepared with a urease concentration of 0.10 g/L using 490 u/mg is 49,000 (u/L) urease enzyme amount. This makes

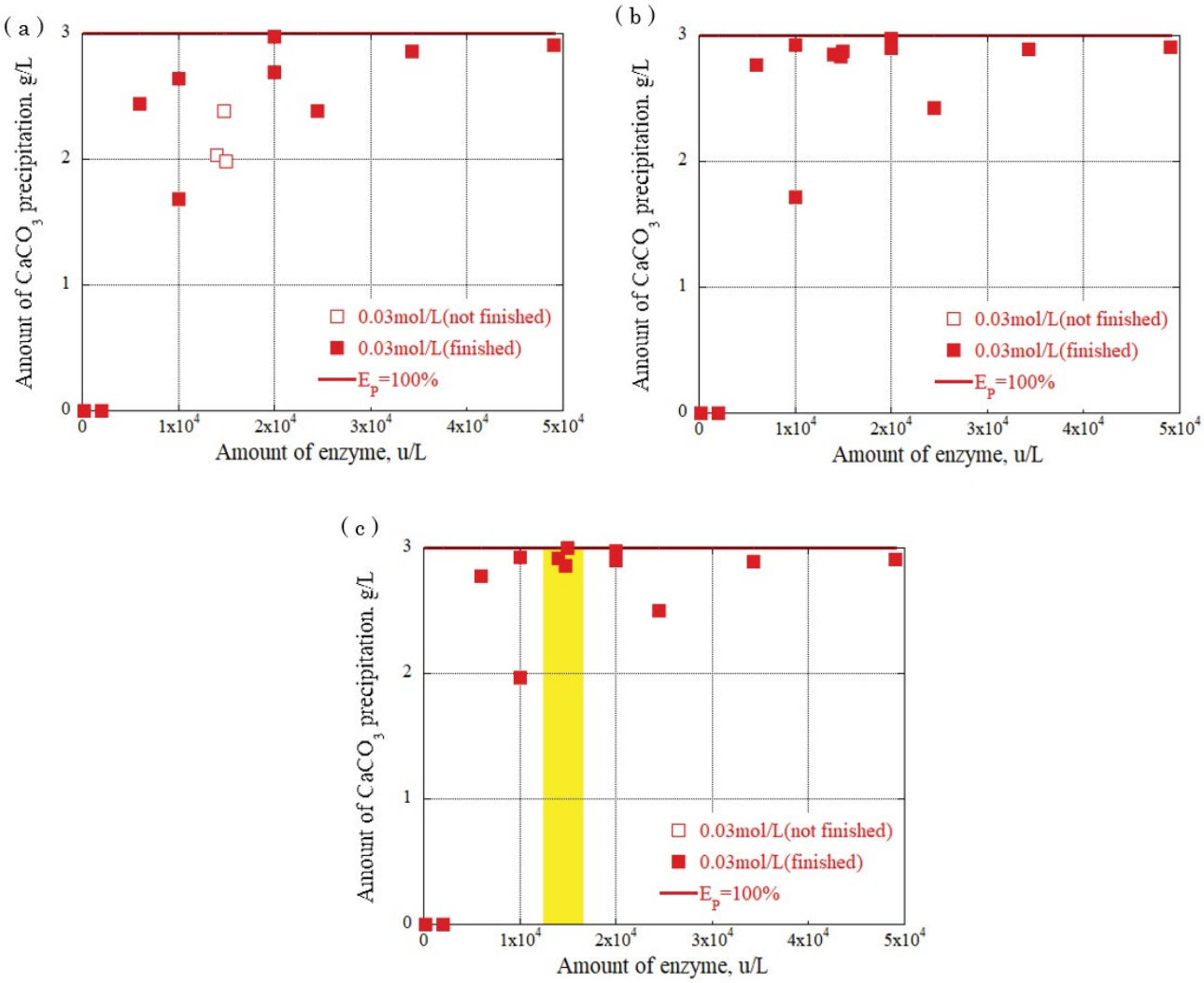

Figure 8: Relationship between urease enzyme amount and $CaCO_3$ amount at urea, calcium chloride concentration: 0.03 mol/L a) $CaCO_3$ precipitation amount after 30 minutes; b) $CaCO_3$ precipitation amount after 90 minutes; c) $CaCO_3$ precipitation amount after 120 minutes.

it possible to unify the two parameters that must be considered: the original enzyme activity of the urease and the urease concentration of the grout material into one parameter, the urease enzyme amount per liter.

The relationship between the urease enzyme amount and the $CaCO_3$ precipitation amount per liter at each time was determined. The results are shown in Figure 8, Figure 9 and Figure 10, providing the urea and calcium chloride concentrations at 0.03 mol/L, 0.09 mol/L, and 0.15 mol/L, respectively. The results are for each hour when the grout material was used. The horizontal axis represents the urease enzyme amount per liter (u/L), the vertical axis represents the $CaCO_3$ precipitation amount per liter (g/L), the open square mark represents the calcium carbonate precipitation continuing, and the solid square mark represents the calcium carbonate precipitation had almost finished. Comparing Figure 8, Figure 9 and Figure 10, the amount of $CaCO_3$ precipitation increased as the amount of urease enzyme per liter increased. The results indicated that the precipitation time increased as the amount of urease enzyme per liter increased. Additionally, there was an optimum amount of enzyme that ensured sufficient calcium carbonate precipitation amount and time. The yellow areas in Figure 8, Figure 9 and Figure 10 are the values corresponding to the optimum amount of enzyme.

Procedure for applying the enzyme-induced precipitation method

The rock samples, accompanied by grout materials, are placed within a vacuum desiccator, creating an environment conducive to the

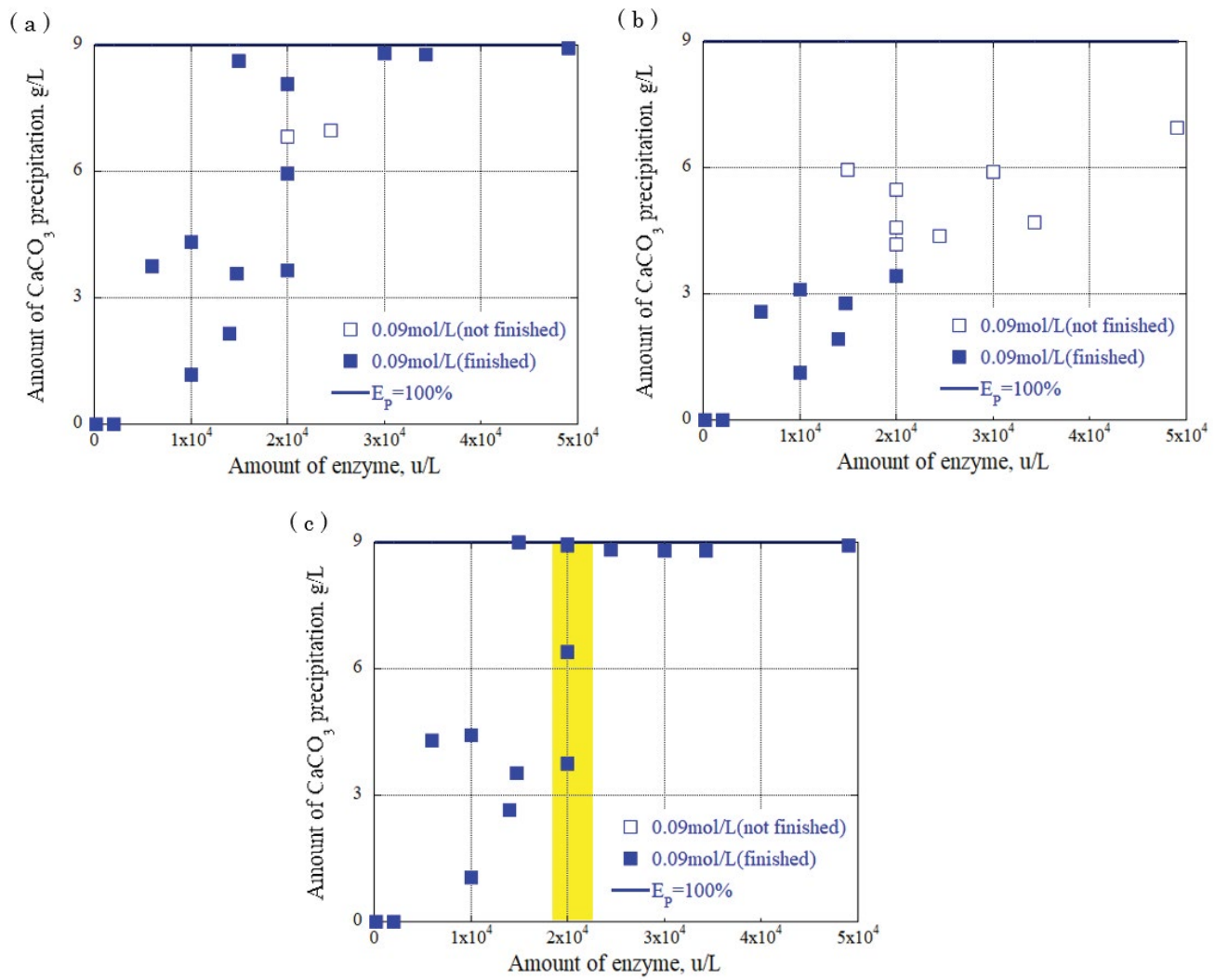

Figure 9: Relationship between urease enzyme amount and $CaCO_3$ precipitation amount at urea, calcium chloride concentration: 0.09 mol/L a) $CaCO_3$ precipitation amount after 30 minutes; b) $CaCO_3$ precipitation amount after 90 minutes; c) $CaCO_3$ precipitation amount after 120 minutes.

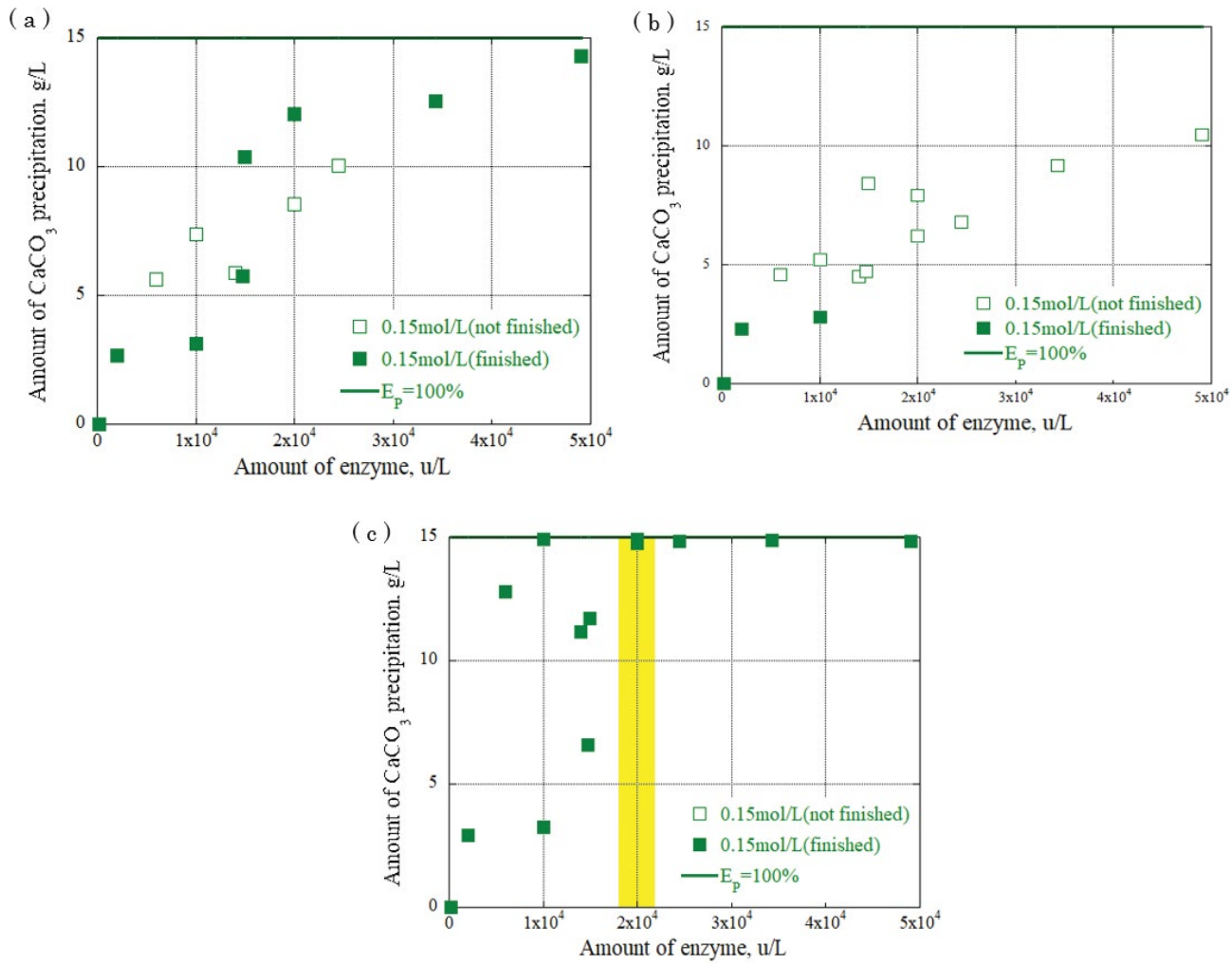

Figure 10: Relationship between urease enzyme amount and $CaCO_3$ precipitation amount at urea, calcium chloride concentration: 0.15 mol / L a) $CaCO_3$ precipitation amount after 30 minutes; b) $CaCO_3$ precipitation amount after 90 minutes; c) $CaCO_3$ precipitation amount after 120 minutes.

infiltration of grout materials into the intricate pore structures of the rocks, and Figure 11 shows a flowchart of the procedure for applying the enzyme-induced calcite precipitation method. First, the mass of the dried rock sample was measured, and then the mineral precipitation method was applied. After approximately 1d, the rock sample was dried in a drying oven, and the mass was measured. Subsequently, the mineral precipitation method was applied again to the same rock sample using grout material under the same application conditions. Similarly, after approximately 1d, it was dried again, and the mass was measured. In this study, the enzyme-induced calcite precipitation method was applied up to three times. The grout material used was 490 u/mg urease, with the solutions prepared with urea and calcium chloride concentrations of 0.03 mol/L, 0.09 mol/L, 0.15 mol/L, and 0.30 mol/L.

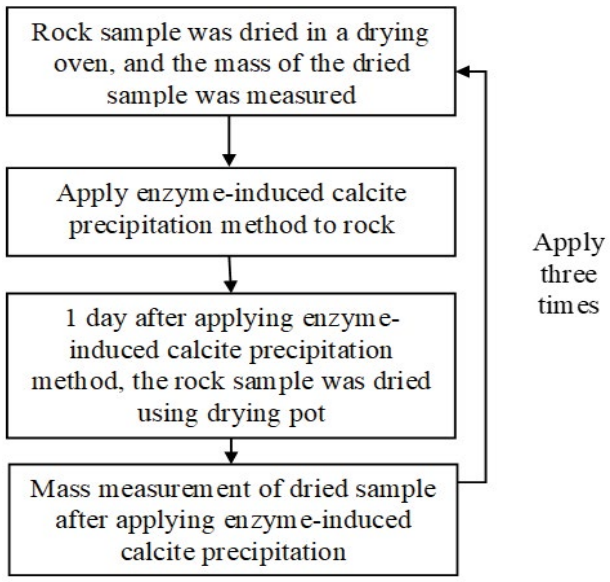

Figure 11: Procedure for applying the enzyme-induced calcite precipitation method.

After the mass measurement was completed, the mass of the dried sample to which the mineral precipitation method was not applied was subtracted from the mass of the dried sample to which the mineral precipitation method was applied, and the $CaCO_3$ precipitation amount in the first application was calculated. Similarly, this process was completed after the second application of the mineral precipitation method. The precipitate was deposited in the voids of the rock sample at each application frequency. Subsequently, the mass of calcium carbonate was calculated. Moreover, it is possible to confirm that during the reaction and after the reaction, exclude calcium carbonate, the other precipitation not existing in the solutions.

One-Dimensional Permeability Test Results

In this study, as described in Chapter 2, a one-dimensional permeability test was conducted to evaluate the effect of the enzyme-induced calcite precipitation method on impermeable properties.

To evaluate the effect of different urea and calcium chloride concentrations on impervious properties, grouting materials were prepared at urea and calcium chloride concentrations of 0.03 mol/L, 0.09 mol/L, 0.15 mol/L, and 0.30 mol/L, and each solution was allowed to penetrate the rock samples. One-dimensional permeability tests were conducted. For urease, two experiments with a urease concentration adjusted to 0.10 g/L and 0.05 g/L using 490 u/mg urease, were performed to elucidate the effect of the difference in the urease concentration in the grout material on the impermeable properties. In addition, after the water permeation test was completed, the sample was dried and the mineral precipitation method was applied again using the same concentration of grout material to increase the amount of calcium carbonate precipitation in the rock sample, and calcium carbonate was increased by increasing the number of applications. The effect of the change in the amount of precipitation on the impermeable properties was evaluated. The enzyme-induced calcite precipitation method was applied up to three times. Figure 12 and Figure 13 show the results of the evaluation of the intrinsic permeability, with the concentrations of calcium chloride and urea in the grout material indicated on the horizontal axis, and the intrinsic permeation rate on the vertical axis. The solid circlered mark in the figure is the evaluation result of the intrinsic permeability when the enzyme-induced calcite precipitation method was applied once, and the solid square blue mark and solid triangle green marks are the evaluation results after applying the enzyme-induced calcite precipitation method twice and three times. Based on the results, for sandstones with a large void diameter and high

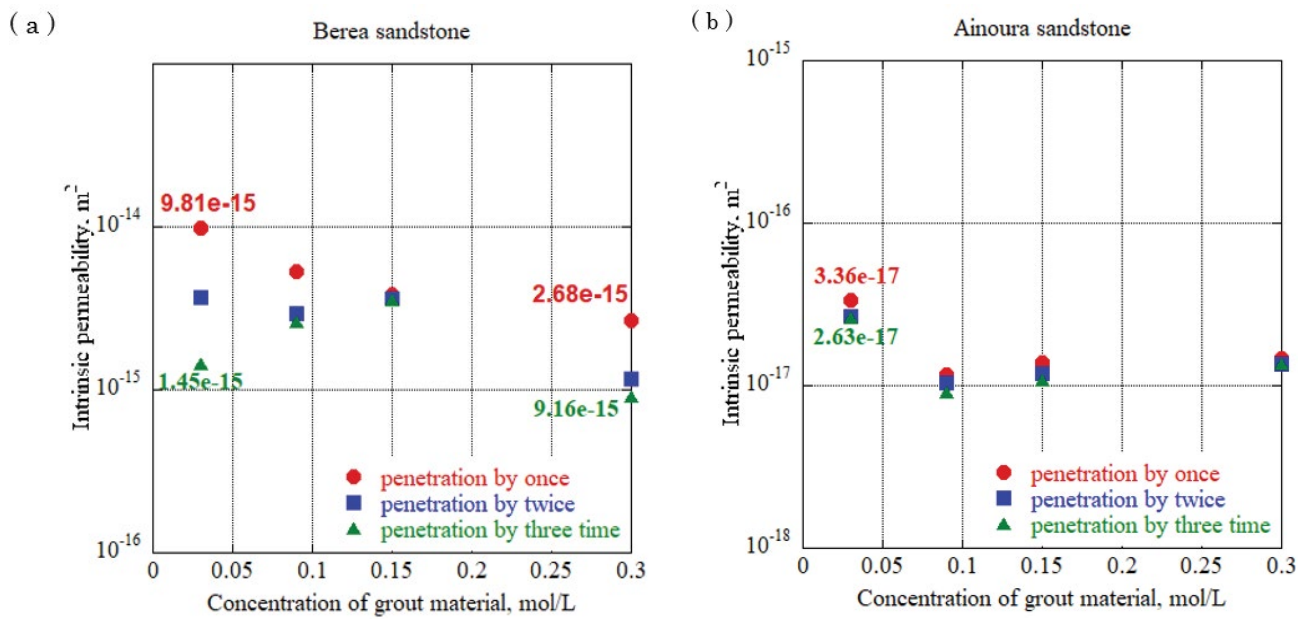

Figure 12: Intrinsic permeability in each rock sample at urease concentration 0.10 g/L, a) Berea sandstone; b) Ainoura sandstone.

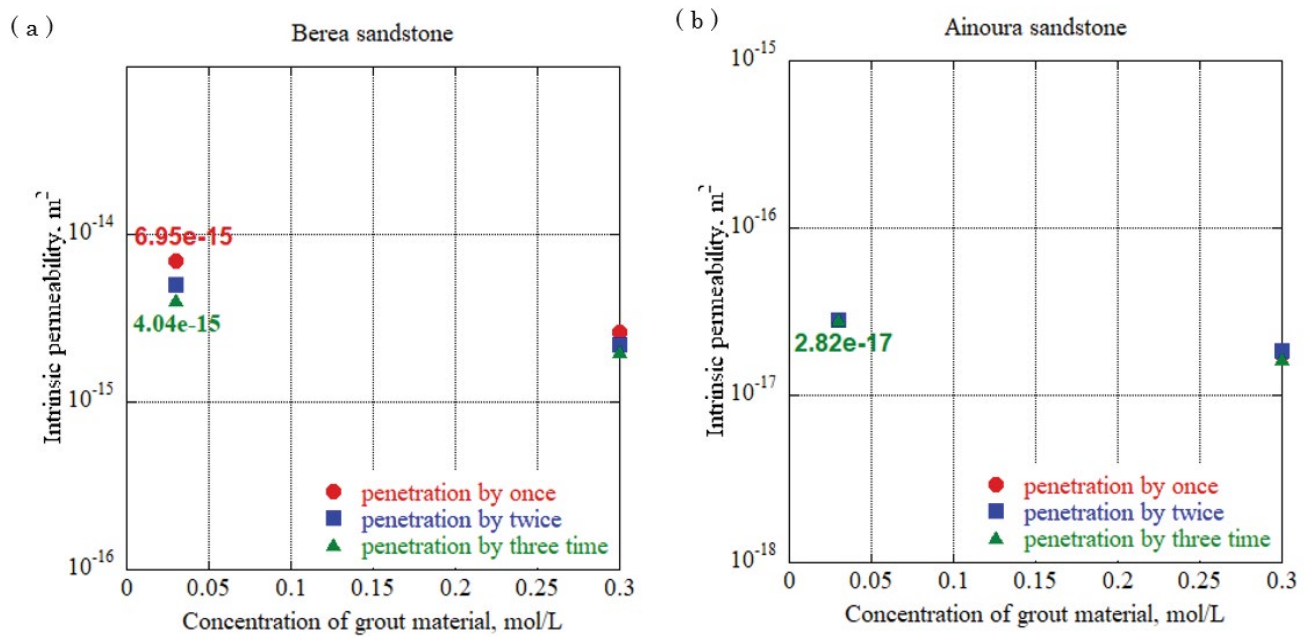

Figure 13: Intrinsic permeability in each rock sample at urease concentration 0.05 g/L, a) Berea sandstone; b) Ainoura sandstone.

intrinsic permeability, such as Berea sandstone, increasing the number of times the mineral precipitation method is applied and using the optimum enzyme concentration can significantly reduce the intrinsic permeability with sufficient precipitation time. During Ainoura sandstone as a rock sample, compared with Berea sandstone it is hard to observe a significant reduction on the intrinsic permeability. For urease concentration 0.1 g/L with 0.03 mol/L concentration of grout material, the permeability reduces from 9.81 × 10^{-15} m^2 to 1.45 × 10^{-15} m^2 which represents from first penetration to third penetration on Berea rock sample, additionally, during same concentration of urease with 0.3 mol/L grout material concentration, the permeability reduces from 2.68 × 10^{-15} m^2 to 9.16 × 10^{-15} m^2. In the case of the Ainoura rock sample, permeability reduces from 3.36 × 10^{-17} m^2 to 2.63 × 10^{-17} m^2, for the 0.05g/L concentration of urease with 0.03 mol/L concentration of grout material, the permeability reduces from 6.95 × 10^{-15} m^2 to 4.04 × 10^{-15} m^2 in the Berea sandstone, the reason that it is hard to observe the significant changes on Ainoura rock sample is that the precipitation hard to infiltrate the internal structure due to narrow pore throat, moreover, after the precipitation method, the materials only occur the surface area of rock sample.

Evaluation of $CaCO_3$ Precipitation Phenomenon via CT Image Analysis

In this study, a bulk evaluation was performed using an industrial X-ray CT scanner to visualize the precipitation of calcium carbonate inside the rock and to quantitatively evaluate the resulting density change. The 490 μ/mg urease was added to the grout material, as in the one-dimensional permeability test.

Bulk evaluation using an industrial X-ray CT scanner

In this study, X-ray CT imaging was performed to visualize the region inside the rock where calcium carbonate was deposited after applying the enzyme-induced calcite precipitation method, and resulting in the density change was quantitatively evaluated. First, the evaluation results of an industrial X-ray CT scanner are performed. For the image analysis using an industrial X-ray CT scanner, the rock samples used were Berea and Ainoura sandstones with a diameter of 30 mm and a height of 20 mm. Table 1 shows the imaging conditions for industrial X-ray imaging.

Image subtraction method and CT image analysis

In a previous study, to extract the density information due to diffusion, an image subtraction

Table 1: Industrial X-ray CT scanner settings conditions.

Settings	Conditions
Voltage	300 kV
Scan area	150 mm
One pixel size	0.073 mm
Slice thickness	0.3 m
Scan mode	Full scan
Matrix size	2048 × 2048
Scan mode	Single
Scan speed	Fine

method was applied to the CT images [32]. In our study, to evaluate the precipitation state using the enzyme-induced calcite precipitation method, using an industrial X-ray CT scanner, a rock sample in a water-saturated state in which the grout material had penetrated one day after the application of the Enzyme Induce Calcite Precipitation method was used. The inter-image difference method is effective for extracting only the amount of change in density and removing the inhomogeneity of the rocks and the noise component inevitably contained in the original CT image. First, *(i, j)* was assigned to each pixel of the CT image, and the CT values at this address are C_p *(i, j)* and CW *(i, j)*. Here, the subscript *P* represents the enzyme-induced calcite precipitation application state and *W* represents the water saturation state. By applying the inter-image difference method, the increment in the CT value at address *(i, j)* could be obtained. *ΔC (i, j)* can be expressed using Equation:

$$\Delta C(i,j) = C_p(i,j) - C_W(i,j)$$

Where *ΔC (i, j)* indicates an increase in the CT value owing to the mineral content deposited inside the rock sample using the enzyme-induced calcite precipitation method. Subsequently, the $CaCO_3$ precipitation rate of the rock sample was calculated from the increment in the obtained CT value. Assuming that the CT value of water in an industrial X-ray CT scanner is CT_{water} and the CT value of calcium carbonate is CT_{CaCO3}, the $CaCO_3$ precipitation rate $\in p(i, j)$ can be calculated using Equation:

$$\in_p(i,j) = \frac{\Delta C(i,j)}{CT_{CaCO_3} - CT_{water}}$$

The CT value of water is known to be 0 in an industrial X-ray CT scanner, therefore, CT_{water} = 0 in the equation. In addition, CT imaging was performed on calcium carbonate alone to calculate the CT value of calcium carbonate, and the average *CT* value was 570. Table 2 lists the conditions for applying the enzyme-induced calcite precipitation method to the rock samples used for evaluation by the industrial X-ray CT scanner. Case 1 used a solution prepared with 0.03 mol/L grout, 0.10 g/L urease, and relatively low concentrations of urea and calcium chloride. Case 2 used a solution prepared with 0.30 mol/L grout, 0.10 g/L urease, and a relatively high concentration of urea and calcium chloride (a concentration 10 times that of Case 1). The mineral precipitation method was applied only once during the evaluation using an industrial X-ray CT scanner. The distribution of the $CaCO_3$ precipitation rate under each application condition is shown in Figure 14, and the calculation results of the $CaCO_3$ precipitation rate are shown in Figure 15. The warm-colored part in Figure 14 demonstrates the area where the density change was large and the $CaCO_3$ precipitation rate was also high. Furthermore, the occurrence of a few areas exhibiting cold colors suggests the presence of noise artifacts in the industrial X-ray CT image. In general, the findings from the CT image analysis confirm calcium carbonate precipitation, with a notable occurrence observed, particularly in the Berea sandstone of Case 1. However, the density change observed in the Berea sandstone of Case 2 was comparatively smaller. This discrepancy can be attributed to the higher concentration of urea and calcium chloride employed in Case 2, and a large amount of calcium carbonate was deposited in the voids near the sample surface before penetrating the rock sample. In the case of the Ainoura sandstone, the density increment did not change much, even when comparing Cases 1 and 2. The limited intrinsic permeability of the Ainoura sandstone contributed to the hindrance of clogging within the voids, as calcium carbonate was deposited near the rock sample's surface before

Table 2: Conditions for applying the enzyme-induce calcite precipitation method to rock samples used for industrial X-ray CT imaging.

	Concentration of urea & $CaCl_2$ [mol/L]	Concentration of urease [g/L]
Case 1	0.03	0.10
Case 2	0.30	0.10

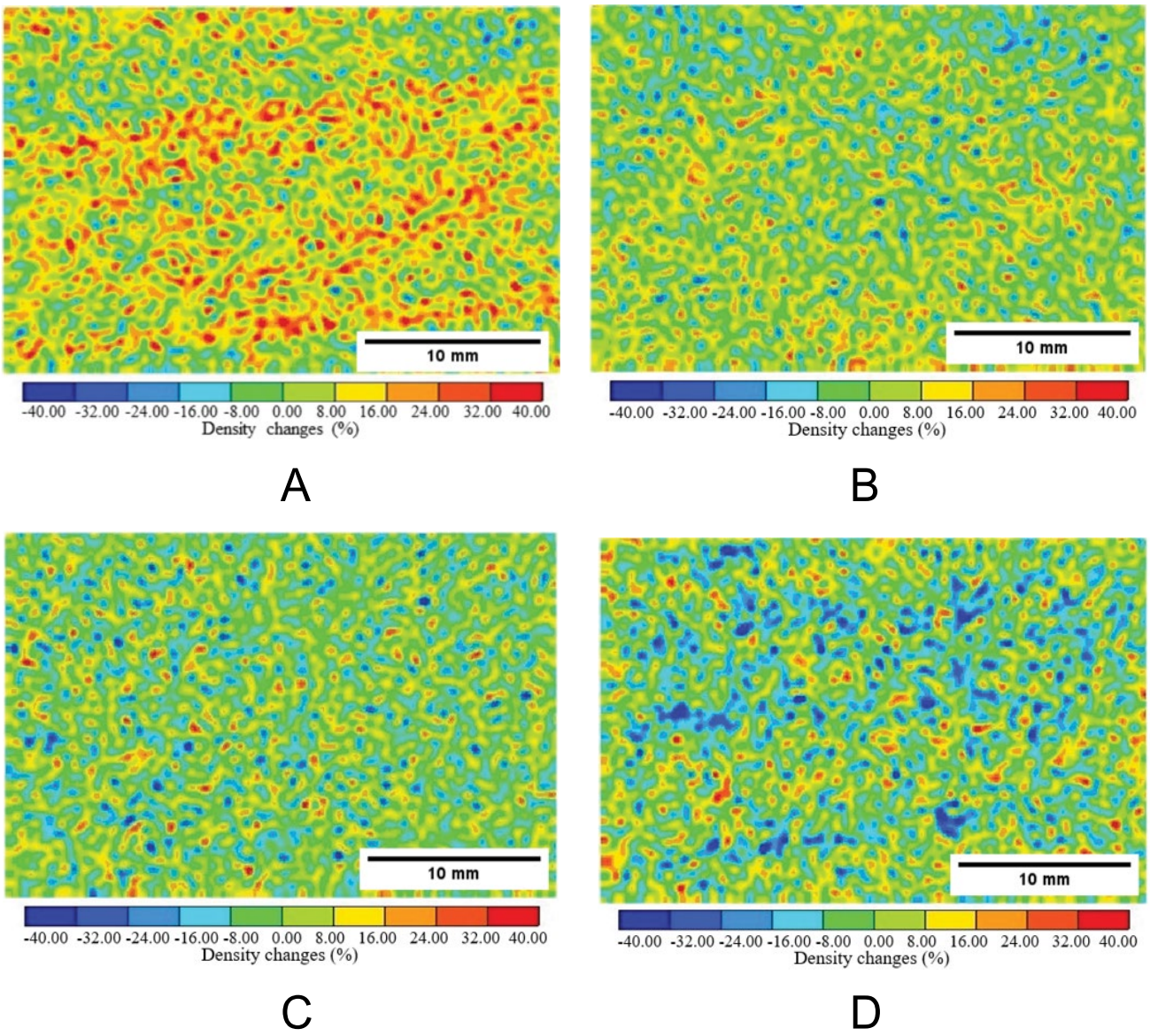

Figure 14: Precipitation rate distribution of calcium carbonate obtained by image subtraction method, a) Berea sandstone-Case 1; b) Berea sandstone-Case 2; c) Ainoura sandstone-Case 1; d) Ainoura sandstone-Case 2.

penetrating the sample. The Ainoura sandstone exhibits high porosity; however, the poor pore connectivity and intrinsic permeability impede the infiltration and precipitation of materials within the rock sample. These factors may explain the difficulty in observing distinct density differences in the precipitated materials.

Figure 15 illustrates the results of comparing the precipitation rates obtained from mass measurements and CT value measurements. It was observed that the $CaCO_3$ precipitation rate calculated from CT values was higher than that calculated from the overall mass measurement of the rock sample. This disparity can be attributed to the resolution limitations of industrial X-ray CT imaging, specifically in the calculation of precipitation rates using CT values. The voxel numbers derived from CT images represent the occurrences of precipitation, but due to inherent noise and low resolution, these values may include areas where precipitation has not taken place. When Case 1 was applied to Berea sandstone, the $CaCO_3$ precipitation rate was higher than that observed in Ainoura sandstone. This trend was consistently observed, indicating a similar pattern in the $CaCO_3$ precipitation rates for both sandstone types.

Results and Discussions

The main objectives of this study were twofold.

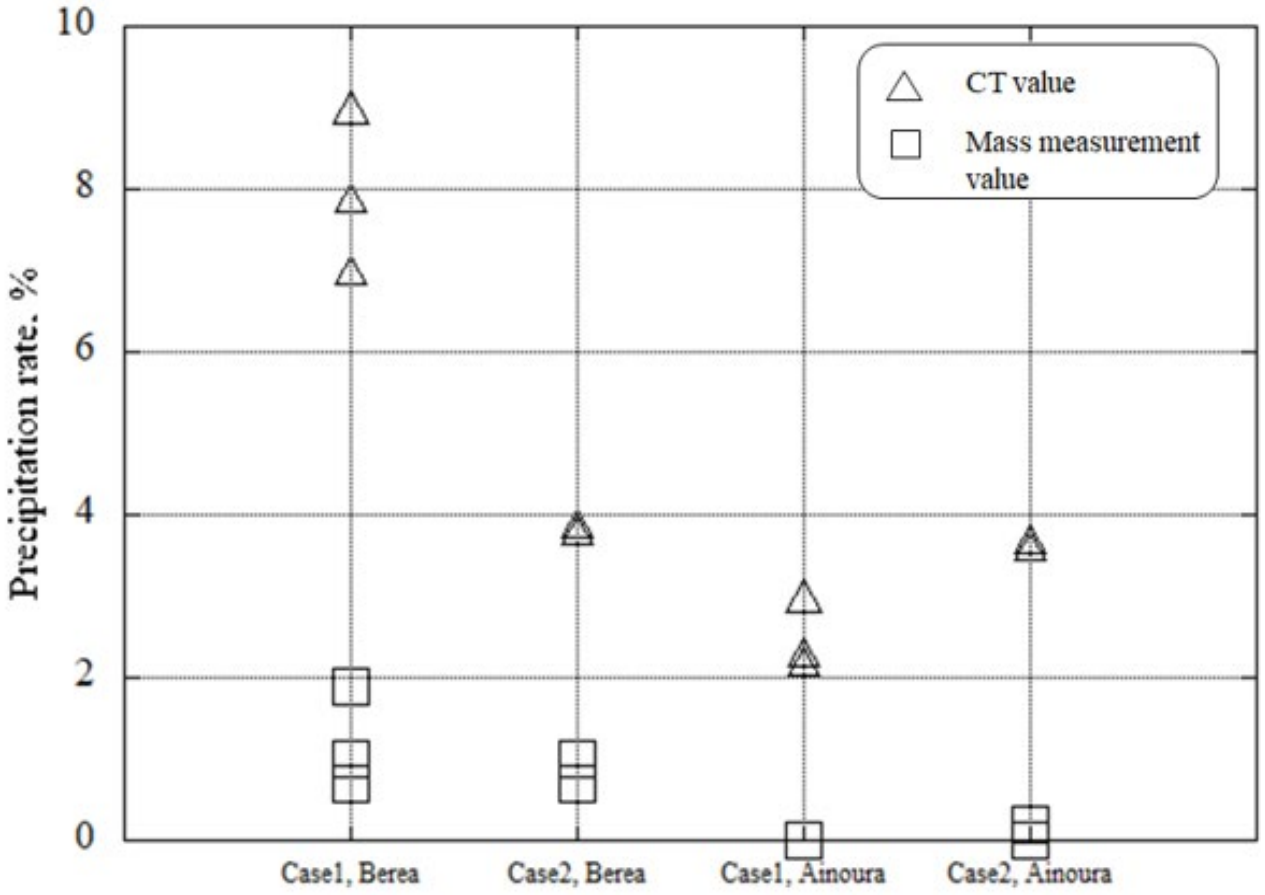

Figure 15: Comparison of $CaCO_3$ precipitation rate obtained by the image subtraction method and $CaCO_3$ precipitation rate obtained by mass measurement.

Firstly, we aimed to explore the most effective mixing design for grouting materials in the enzyme-induced calcite precipitation (EICP) method. Secondly, we sought to quantitatively assess the impact of this method on enhancing impermeability by effectively blocking pores within the rock.

The results indicate that a significant value was achieved after 120 minutes, signifying the completion of the chemical reaction. Notably, the combination of 0.03 mol/L urea and calcium chloride produced the highest amount of precipitation, approximately 3 g/L, with 1.5×10^4 u/L enzyme concentration. For the combination of 0.09 mol/L urea and calcium chloride, a range of precipitation amounts was observed with 2×10^4 u/L enzyme concentration: 4 g/L, 7 g/L, and 9 g/L. The highest amount of precipitation, 15 g/L, was obtained with the combination of 0.15 mol/L urea and calcium chloride and 2×10^4 u/L enzyme concentration, surpassing other urea and calcium chloride combinations. These findings underscore the influence of enzyme concentration and the combination of urea and calcium chloride on the amount of precipitation generated during precipitation. During the one-dimensional permeability test, the results indicated a significant decrease in the permeability of the Berea sandstone. The number of applications had a substantial effect on the intrinsic permeability. The combination of urea and urease at 0.03 mol/L and 0.15 mol/L decreased the permeability from 10^{-14} m^2 to 10^{-15} m^2 after three applications of the enzyme-induced calcite precipitation method. In the Ainoura sandstone, a significant decrease in permeability was not observed after the application of Enzyme -Induced Calcite precipitation method. The main reason is that the physical properties of the Ainoura samples' internal structures, which have poor permeability, prevented the infiltration of the rock samples. In a bulk evaluation using an industrial X-ray CT scanner, the results indicated that compared with the Ainoura sandstone, considerable precipitation was observed in the

Berea sandstone with relatively low concentrations of urea and calcium chloride. The concentration of urease played a crucial role in the enzyme-induced calcite precipitation process. In both Berea and Ainoura sandstone, density differences were observed following the application of enzyme-induced calcite precipitation using various concentrations of urease, regardless of the concentrations of urea and calcium chloride. This can be attributed to the deposition of a large number of precipitated materials on the surface of the rock samples at high concentrations of urea and calcium chloride, hindering the penetration of the grout materials into the rock samples.

These results provide valuable insights into the application of the enzyme-induced calcite precipitation method on conservational rock engineering. However, the noise of industrial X-ray CT scanner images generated few data misleading results, such as the blue pattern on the subtracted image, importantly, during further studies, we will use advanced high-resolution X-ray CT scanners such as μ-Focused X-ray CT scanners to visualize the internal pore structure of rock sample also investigations are required to explore the long-term durability and stability of the calcite precipitation and the impact on the overall machinal properties of the rock samples.

Conclusion

In this study, we focused on calcium carbonate, which is an insoluble crystal, and introduced a method called enzyme-induced calcite precipitation to improve its water-shielding property, with a particular focus on its relevance to carbon capture and storage (CCS) initiatives. By utilizing different concentrations of urea, calcium chloride, and urease, we evaluated the precipitation time and amount of precipitation in Berea sandstone and Ainorua sandstone. The visualizations obtained through an industrial X-ray CT scanner revealed significant precipitation within the Berea sandstone, while the Ainoura sandstone exhibited comparatively less precipitation. The subsequent one-dimensional permeability tests provided quantitative assessments of the water-shielding properties. The application of the EICP method led to a notable decrease in the intrinsic permeability of both Berea and Ainoura sandstones. However, the reduction was more pronounced in the Berea sandstone, which exhibited a decrease of approximately 1/10 in intrinsic permeability after three applications of EICP. In contrast, the Ainoura sandstone showed minimal changes in intrinsic permeability with varying application numbers. These findings demonstrate the potential of EICP as an effective approach for enhancing water-sealing capabilities in geotechnical and environmental applications. Moreover, the study highlights the benefit of carbon sequestration within the rock formations, aligning with efforts to mitigate climate change and reduce greenhouse gas emissions.

Acknowledgments

This work was supported by JST SPRING, Grant Number JPMJSP2127 (Kumamoto University Cross-disciplinary Doctoral Human Resource Development Program to Lead the Well-being Society).

References

1. Baklid A, Korbol R, Owren G (1996) Sleipner vest CO_2 disposal, CO_2 injection into a shallow underground aquifer. SPE Annual Technical Conference and Exhibition 269-277.
2. Eigel PZ, Arts R, Lothe AE, Lindeberg EB (2004) Reservoir geology of the Utsira Formation at the first industrial-scale underground CO_2 storage site (Sleipner area, North Sea). Geological Society 233: 165-180.
3. Furre K, Eiken O, Alnes H, Vevatne JN, Kiar AF (2017) 20 years of monitoring CO_2-injection at Sleipner. Energy Procedia 114: 3916-3926.
4. Manuilova A, Koiwanit J, Piewkhaow L, Wilson M, Chan CW, et al. (2014) Life Cycle Assessment of Post-combustion CO_2 Capture and CO_2-Enhanced oil recovery based on the boundary dam integrated carbon capture and storage demonstration project in Saskatchewan. Energy Procedia 63: 7398-7407.
5. Akerboom S, Waldmann S, Mukherjee A, Agaton C, Sanders M, et al. (2021) Different this time? The prospects of CCS in the Netherlands in the 2020s. Front Energy Res 9: 644796.
6. Kundu N, Sarkar S (2020) Porous organic frameworks for carbon dioxide capture and storage. Journal of Environmental Chemical Engineering 9: 105090.
7. Cook PJ (2009) Demonstration and deployment of carbon dioxide capture and storage in Australia. Energy Procedia 1: 3859-3866.
8. Dahowski RT, Li X, Davidson CL, Wei N, Dooley JJ (2009) Regional opportunities for carbon dioxide capture and storage in China: A comprehensive CO_2

storage cost curve and analysis of the potential for large-scale carbon dioxide capture and storage in the People's Republic of China. PNNL-19091.

9. Dymochkina MG, Samodurov MS, Pavlov VA, Penigin AV, Ushimaev OS (2021) Geological potential of carbon dioxide capture and storage of the Russian Federation (Russian). OIJ 12: 20-23.

10. Andrew CM, Kund D, Lee HS, Alfred BC, Robin G (2010) Microbially enhanced carbon capture and storage by mineral-trapping and solubility-trapping. Environ Sci Technol 44: 5270-5276.

11. Franklin MOJ (2009) CO_2 capture and storage: Are we ready? Energy Environ Sci 2: 449-458.

12. Spigarelli BP (2013) A novel approach to carbon dioxide capture and storage. Michigan Technological University.

13. Mendoza EYM, Drozd V, Durygin A, Saxena SK (2020) Methods for carbon dioxide capture. United States Patent 16: 569.

14. Mitchell C, Dideriksen K, Spangler LH, Cunningham AB, Gerlach R (2010) Microbially enhanced carbon capture and storage by mineral-trapping and solubility-trapping. Environ Sci Technol 44: 5270-5276.

15. Phillips J, Lauchnor E, Eldring JJ, Esposito R, Mitchell AC, et al. (2012) Potential CO_2 leakage reduction through biofilm-induced calcium carbonate precipitation. Environ Sci Technol 47: 142-149.

16. Krajewska B (2018) Urease-aided calcium carbonate mineralization for engineering applications: A review. Journal of Advanced Research 13: 59-67.

17. Heriansyah P, Hideaki Y, Erizal, Sutoyo, Muhammad F (2020) Review of enzyme-induced calcite precipitation as a ground-improvement technique. Infrastructures 5: 66.

18. Abdullah A, Mohammed LA, Arif AAB, Kehinde L (2021) State-of-the-art review of the applicability and challenges of Microbial-Induced Calcite Precipitation (MICP) and Enzyme-Induced Calcite Precipitation (EICP) techniques for geotechnical and geoenvironmental applications. Crystals 11: 370.

19. Isaac A, Mizanur R, Rajibul K, Simon B (2021) Enzyme-induced calcium carbonate Precipitation and its engineering application: A Systematic review and meta-analysis. Construction and Building Materials 308: 125000.

20. Zeeshan T, Mohamed M, Manar A, Mohamad B, Abdul N (2022) Lost circulation mitigation using modified enzyme-induced calcite precipitation technique. Petroleum Science and Engineering 210: 110043.

21. Baker DR, Mancini L, Polacci M (2012) An introduction to the application of X-ray microtomography to the three-dimensional study of igneous rocks. Lithos 148: 262-276.

22. Ahmed MR, Yasmin J, Collins W, Cho BK (2018) X-ray CT image analysis for the morphology of muskmelon seed in relation to germination. Biosystems Engineering 175: 183-193.

23. Shou Y, Zhao Z, Zhou X (2020) Sensitivity analysis of segmentation techniques and voxel resolution on rock physical properties by X-ray imaging. Journal of Structural Geology 133: 103978.

24. Choi CS, Lee YK, Song JJ (2020) Equivalent pore channel model for fluid flow in rock based on microscale X-ray CT Imaging. Materials 13: 2619.

25. Alhammadi AM, Gao Y, Akai T, Blunt MJ, Bokeljic B (2020) Pore-scale X-ray imaging with measurement of relative permeability, capillary pressure and oil recovery in a mixed-wet micro-porous carbonate reservoir rock. Fuel 268: 117018.

26. Zandomeneghi D, Voltolini M, Mancini L, Brun F, Dreossi D, et al. (2010) Quantitative analysis of X-ray microtomography images of geomaterials: Application to volcanic rocks. Geosphere 6: 793-804.

27. Wang X, Pan J, Wang K, Ge T, Wei J, et al. (2020) Characterizing the shape, size, and distribution heterogeneity of pore-fractures in high rank coal based on X-ray CT image analysis and mercury intrusion porosimetry. Fuel 282: 118754.

28. Jiang L, Song Y, Yang M, Xue Z, Zhao Y, et al. (2015) Application of X-ray CT investigation of CO_2-brine flow in porous media. Experiments in Fluid 56: 91.

29. Bagudu U, McDougall SR, Mackay EJ (2015) Pore-to-core-scale network modelling of CO_2 migration in porous media. Transport in Porous Media 110: 41-79.

30. Ahkami M, Parmigiani A, Palma PR, Saar MO, Kong XZ (2019) Study on mineral precipitation in fractured porous media using lattice Boltzmann methods. European Geothermal Congress, The Netherlands.

31. Yang FC, Stack AG, Starchenko V (2021) Micro-continuum approach for mineral precipitation. Sci Rep 11: 3495.

32. Sato A, Yatsunami T, Ikeda K, Tsuda K, Fukumitsu T, et al. (2016) Pore-scale analysis of diffusion phenomena in rocks by means of u-focus X-ray CT. Journal of the Society of Materials Science 65: 451-456.